JOURNAL OF SYNCHROTRON RADIATION

ISSN 1600-5775

Received 19 December 2018
Accepted 15 March 2019

Edited by M. Yamamoto, RIKEN SPring-8 Center, Japan

**Keywords:** microtomography; phase contrast tomography; STXM; ovary.

**Supporting information**: this article has supporting information at journals.iucr.org/s

# Hard and soft X-ray imaging to resolve human ovarian cortical structures

Lorella Pascolo,[a]* Gabriela Sena,[b] Alessandra Gianoncelli,[c]* Alice Cernogoraz,[d] Geroge Kourousias,[c] Brian D. Metscher,[e] Federico Romano,[a] Gabriella Zito,[a] Serena Pacilè,[c] Regina Barroso,[f] Giuliana Tromba,[c] Marina Zweyer[d] and Giuseppe Ricci[a,d]

[a]Institute for Maternal and Child Health, IRCCS Burlo Garofolo, 34147 Trieste, Italy, [b]Nuclear Engineering Institute, Federal University of Rio de Janeiro, Rio de Janeiro 21941-594, Brazil, [c]Elettra Sincrotrone Trieste, SS 14 km 163.5 in Area Science Park, Basovizza, 34149 Trieste, Italy, [d]Department of Medical, Surgical and Health Sciences, University of Trieste, 34149 Trieste, Italy, [e]Department of Theoretical Biology, University of Vienna, Vienna, Austria, and [f]Physics Institute, State University of Rio de Janeiro (UERJ), Rio de Janeiro 21941-594, Brazil.
*Correspondence e-mail: lorella.pascolo@gmail.com, alessandra.gianoncelli@elettra.eu

Laboratory and synchrotron X-ray tomography are powerful tools for non-invasive studies of biological samples at micrometric resolution. In particular, the development of phase contrast imaging is enabling the visualization of sample details with a small range of attenuation coefficients, thus allowing in-depth analyses of anatomical and histological structures. Reproductive medicine is starting to profit from these techniques, mainly applied to animal models. This study reports the first imaging of human ovarian tissue where the samples consisted of surgically obtained millimetre fragments, properly fixed, stained with osmium tetroxide and included in epoxydic resin. Samples were imaged by the use of propagation phase contrast synchrotron radiation micro-computed tomography (microCT), obtained at the SYRMEP beamline of Elettra light source (Trieste, Italy), and X-ray absorption microCT at the Theoretical Biology MicroCT Imaging Laboratory in Vienna, Austria. The reconstructed microCT images were compared with the soft X-ray absorption and phase contrast images acquired at the TwinMic beamline of Elettra in order to help with the identification of structures. The resulting images allow the regions of the cortex and medulla of the ovary to be distinguished, identifying early-stage follicles and visualizing the distribution of blood vessels. The study opens to further application of micro-resolved 3D imaging to improve the understanding of human ovary's structure and support diagnostics as well as advances in reproductive technologies.

## 1. Introduction

The improved visualization and clear understanding of human ovary's structures is highly desirable to support diagnostics as well as advances in reproductive technologies (Paulini *et al.*, 2017). Several works have been reported in the literature concerning the ovary anatomy resolved at high resolution (Bukovsky *et al.*, 2004); however, conventional examinations are usually performed with two-dimensional techniques such as visible light and transmission electron (TEM) microscopies (Makabe *et al.*, 2006). Ultrasound is normally used for clinical purposes, usually to help finding anatomical modifications like ovarian neoplasia, cysts and antral follicles, whose diameters exceed 400 µm. However, primordial, primary, secondary and little antral follicles are too small to be seen with ultrasounds (Williams & Erickson, 2000). Computed tomography (CT) is often used for monitoring and diagnosing cysts and tumours in ovaries (Paulini *et al.*, 2017; Rozenblit *et al.*, 2001; Saksouk &

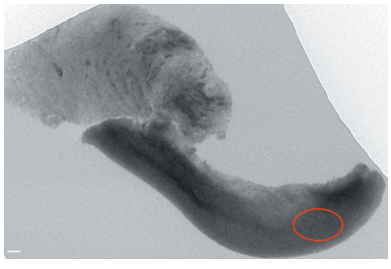

Johnson, 2004), but the resolution offered by clinical CT instruments is not high enough to resolve details of the follicles. The possibility of resolving this type of tissue in a three-dimensional (3D) visualization with micrometre resolution is of paramount importance for a comprehensive understanding not only of its morphology but also its physiology. Such a methodology could be useful for comparing ovarian fragments before and after freezing, in the context of autotransplantation of ovarian tissue after a chemo or a radio-therapeutic treatment, which are highly gonadotoxic (Ladanyi *et al.*, 2017). Moreover, this could provide new insights on the recent perspective of developing a transplantable artificial ovary. To date, a lot of artificial ovary prototypes have been created (Chiti, Dolmans, Donnez *et al.*, 2017; Amorim & Shikanov, 2016; Laronda *et al.*, 2017) with impressive results, mostly with mice follicles; however, human follicles seem to have different requirements. A better knowledge of the human ovarian three-dimensional structure could help in creating an artificial ovary more similar to the native one and thus more efficient (Chiti, Donnez *et al.*, 2018; Chiti, Dolmans, Hobeika *et al.*, 2017; Chiti, Dolmans *et al.*, 2018).

Microcomputed tomography (microCT) is established as a non-destructive imaging tool for the production of high-resolution 3D images of various types of samples. Numerous reviews of the development and applications of microCT have been published (Ritman, 2011; Boerckel *et al.*, 2014). In conventional X-ray microCT, contrast is due to the differences in absorption within the sample, which depend upon the object thickness and its atomic number and density. For studies on materials made up of low-$Z$ elements like most biological samples, the absorption in the hard X-ray region is weak. This is one of the major drawbacks of the conventional absorption-based X-ray imaging techniques.

Since the 1990s, an alternative approach has been offered using phase-contrast imaging techniques, which can provide improved image contrast (Davis *et al.*, 1995; Wilkins *et al.*, 1996) overcoming the intrinsic limitation of conventional absorption imaging. These techniques, exploiting the spatial coherence of the source, are based on the detection of phase shifts occurring in the X-ray wavefield crossing the samples (Fitzgerald, 2000). Synchrotrons provide X-ray beam with a high degree of coherence and therefore they are the ideal sources for the implementation of these techniques (Cloetens *et al.*, 1996; Arfelli *et al.*, 1998), either for planar imaging or computed tomography (Mayo *et al.*, 2003; Betz *et al.*, 2007). Among the different phase-sensitive approaches (Bravin *et al.*, 2013), the propagation-based technique has the simplest implementation as it uses free-space propagation to encode the phase signal into measured intensities; in general the phase effects are dependent upon the degree of coherence of the incoming beam (related to the source size and the source-to-sample distance), the detector resolution (related to the sample-to-detector distance) and the propagation distances from source to sample and sample to detector (De Caro *et al.*, 2008; Pogany *et al.*, 1997).

Either a conventional laboratory source or a synchrotron source can be used for microCT. Laboratory sources typically produce polychromatic beams emitted in a cone-beam geometry; scans are performed by rotating the sample around a given axis over 180° or 360°, while different projection images are acquired for equally spaced angles. During recent years, microCT using laboratory sources has seen an increasing use in biological and medical research areas with the development of the staining methods (Metscher, 2009), proving to be a powerful technique for biomedical studies. Recent advanced synchrotron and laboratory studies reported also investigations of whole ovaries of laboratory animals (Kim *et al.*, 2012; Paulini *et al.*, 2017) and bovines (Corral *et al.*, 2018), demonstrating the potentialities of this approach for estimating ovarian reserve or analysing tissue changes in a 3D perspective. However, to the best of our knowledge, there is no literature reporting X-ray microCT of human ovarian tissue, likely in part because of the difficulty in accessing human material for research purposes.

In the present study, we report the first imaging of human ovarian tissue by the use of propagation phase contrast (PC) synchrotron radiation (SR) microCT, obtained at the SYRMEP beamline (Tromba *et al.*, 2010) of the Elettra (Trieste, Italy) synchrotron laboratory, and X-ray absorption microCT at the Theoretical Biology MicroCT Imaging Laboratory in Vienna, Austria. The reconstructed microCT images were compared with the soft X-ray absorption and phase contrast images acquired at the TwinMic beamline (Gianoncelli, Kourousias, Merolle *et al.*, 2016) of the Elettra light source in order to help with the identification of structures.

The results show the potentials of microCT and scanning transmission X-ray microscopy (STXM) imaging for distinguishing the regions of cortex and medulla, identifying follicles and visualizing the distribution of blood vessels.

## 2. Materials and methods

### 2.1. Sample preparation

The ovarian tissues were obtained from two patients (ages 37 and 34) undergoing laparoscopic surgery of total or partial oophorectomy, for benign gynaecological conditions, at the Gynaecological and Obstetrics Department of the Institute of Maternal and Child Health IRCCS Burlo Garofolo, Trieste, Italy. The research was approved by the Institutional Review Board of IRCCS Burlo Garofolo. The bioptic samples were collected after obtaining the informed consent from the patients. The biopsies were instantly immersed in 20 ml of flushing medium with heparin at 37°C and then transferred in a culture dish containing flushing medium. The cortical part was manually separated from the medullar portion and cut into small segments (2 mm thickness, 1–2 mm width). The slices were immediately fixed in 2.5% glutaraldehyde (Electron Microscopy Sciences, Hatfield, PA, USA) in 0.1 *M* sodium cacodylate buffer (pH 7.2–7.4) for 3 h at 4°C, then 1 h at room temperature and washed in the same buffer three times for 30 min. A post-fixation treatment was performed with osmium tetroxide 1% in cacodylate buffer 0.1 *M* for 2 h

Table 1
Techniques summary.

| Technique | Instrumentation | Energy (keV) | Resolution (μm) | Field of view | Acquisition time per scan (h) |
|---|---|---|---|---|---|
| MicroCT | Theoretical Biology MicroCT Imaging Lab | 34 | 5 | 3 mm × 3 mm | 0.5 |
| SR-PC microCT | SYRMEP at Elettra | 22 | 2 | 3 mm × 3 mm | 0.5 |
| STXM (2D) | TwinMic at Elettra | 1 | 0.25 | 80 μm × 80 μm | 1 |

at 4°C followed by three washes in the same buffer. The samples were then dehydrated with increasing concentration of ethanol: 50%, 70%, 90% and 100%. Finally, the tissue samples were embedded in epoxy resin (DurcupanTM Fluka) by incubating for three days at 60°C (Pascolo, Venturin, Gianoncelli, Bortul *et al.*, 2018).

For microCT measurements the entire tissues segments were used, while, for X-ray microscopy analyses at the TwinMic beamline, 1.5 μm-thick slices were obtained from the tissue segments and deposited on 4 μm-thick ultralene foils (SPEX SamplePrep, LLC), following the sample preparation described in the literature (Pascolo, Venturin, Gianoncelli, Bortul *et al.*, 2018; Pascolo, Venturin, Gianoncelli, Salomé *et al.*, 2018).

### 2.2. Microtomography

In this work, laboratory absorption-based microCT imaging was performed at the Theoretical Biology MicroCT Imaging Lab at the University of Vienna. The microCT scanning system used for the measurements was an Xradia (Zeiss) MicroXCT-200 (https://www.zeiss.com/microscopy/int/X-ray.html), able to perform tomographic imaging of biological objects of size from about 13 mm down to less than 500 μm in diameter, with spatial resolutions down to 2 μm. This system uses a sealed microfocus X-ray source (Hamamatsu L9421-02, tungsten transmission target with a nominal spot size of 5–7 μm) and secondary optical magnification: each of four scintillator detectors is coupled to an optical microscope objective (1×, 4×, 10×, 20×) to allow variable image resolution by switching objective lenses. The source was operated at 60 kV voltage and 83 μA current, delivering a polychromatic energy spectrum with an average energy of 34 keV. Using an optical magnification of 4×, the image pixel size was 5 μm. Tomographic reconstructions were made using the *XMReconstructor* software supplied with the Xradia system, and initial visualization and rendering of reconstructed microCT images was carried out using *XM3DViewer*.

Phase-contrast microCT scans were performed in the propagation-based modality using the set-up available at the SYRMEP beamline (Tromba *et al.*, 2010) of the Elettra synchrotron facility.

A lens-coupled CCD camera system designed to achieve up to 2.0 μm spatial resolution was used in white X-ray beam mode, with an average energy of 22 keV. The sample-to-detector distance was set to 15 cm. For our experiments, 1440 radiographic projections were acquired over an angular range of 180°. The microtomographic slices are reconstructed from a series of 2D projection images acquired by performing a rotational scan over 180°, which is a very straightforward process compared with serial sectioning (Mizutani *et al.*, 2010). Tomographic slices were reconstructed using the conventional filtered back projection algorithm using the *SYRMEP TOMO PROJECT* (*STP*) software developed by the SYRMEP team (Brun *et al.*, 2015). The approach to the inverse problem of phase retrieval based on the transport-of-intensity (TIE) algorithm (Paganin *et al.*, 2002) was used. Image processing of the 3D volume was carried out using *Avizo* software.

### 2.3. STXM imaging

The tissue slices were analysed at the TwinMic soft X-ray microscopy beamline (Elettra Sincrotrone Trieste, Trieste, Italy) (Gianoncelli, Kourousias, Altissimo *et al.*, 2016). For this experiment, TwinMic was operated in scanning mode, where the sample is raster-scanned under a microprobe delivered by a zone plate (ZP) diffractive optic (Gianoncelli, Kourousias, Altissimo *et al.*, 2016). A fast-readout CCD camera (Andor iXonDV860) downstream of the sample produces absorption and phase contrast images, providing morphological information on the scanned areas (Gianoncelli *et al.*, 2006; Morrison *et al.*, 2006). For these measurements, an incident photon energy of 1 keV and a 600 μm-diameter Au ZP with an outermost zone of 50 nm were used, producing a spot size of 250 nm in diameter on the sample plane, similar to that used by Pascolo, Venturin, Gianoncelli, Salomé *et al.* (2018).

All the experimental conditions used in the measurements are summarized in Table 1.

## 3. Results and discussion

### 3.1. Laboratory microCT

Resin included ovarian tissue blocks of about 2–3 mm in diameter and 2 mm in height were analysed. The reconstruction of the samples from patient 1 (34 years old) is shown in the supporting information (Video S1). In Fig. 1 we report a transversal slice from the tomographic analyses that allows easy identification of the two organ components of the ovary: the medulla part (top left) and the cortical component (bottom right) are clearly distinguished thanks to the different osmium staining according to the tissue composition. Like in most species, human ovaries are composed of an outer cortex and inner medulla. The medulla is composed of loose areolar connective tissue containing numerous elastic and reticular fibres (extracellular matrix), large blood vessels and lymphatic structures. In Fig. 1, the many vessel walls are particularly visible because of the high contrast due to osmium staining of phospholipids. The cortex of ovaries is normally composed of

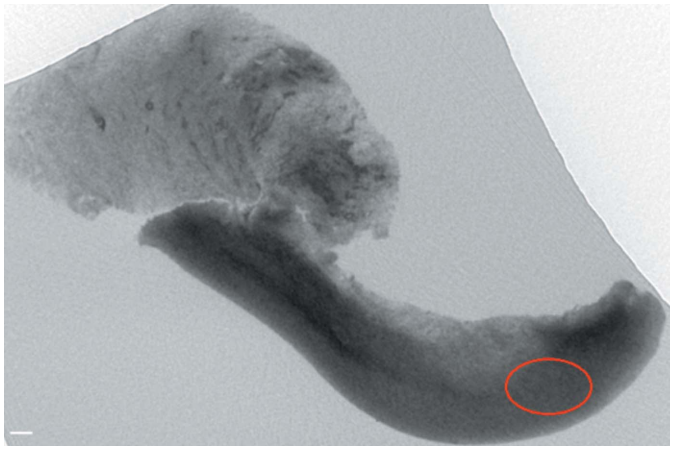

**Figure 1**
Transversal slice from laboratory microCT allowing to easily identify the two organ components of the ovary: the medulla part (top left) and the cortical component (bottom right). Scale bar: 50 µm. The red oval indicates the region from where Fig. 2 was extracted.

ovarian follicles and stromal elements, with small vessels. The hyperdense part (bottom right of the image) corresponds to the ovarian cortex, which is known to be denser than the medulla (top left).

Ovarian follicles can be found at different stages of development (least mature to most mature): primordial, primary, secondary, secondary-vesicular and mature. However, the age of the patient is compatible with low ovarian reserve, thus small numbers of follicles at all stages.

Interestingly, when inspecting the CT reconstruction of the whole tissue sample, we identified a cortical primary ovarian follicle having a diameter of 35–37 µm: Fig. 2 shows a series of consecutive slices extracted from the CT reconstruction every 5 µm. The follicle is clearly recognizable from the lower absorption of the ooplasm compared with the surrounding stromal tissue, and from the presence of the central denser part corresponding to the nucleus of the follicle. The CT spatial resolution does not allow the maturation stage of the follicle to be defined; however, its dimensions suggest a primordial or primary stage.

### 3.2. Synchrotron microCT

At SYRMEP we imaged a resin-embedded tissue slice of 2 mm diameter × 2 mm height from patient 2 (age 37), and the construction of a 0.7 mm diameter × 1 mm high segment is provided in the supporting information (Video S2).

Fig. 3 shows a transversal section of that sample. The tissue contrast is well enhanced by the osmium staining and at this resolution one can perceive the occurrence of vascular structures, which are particularly highly dense in the lumen border, and hints at the presence of stromal cells (arrows). Fig. S1 of the supporting information shows an additional slice representing a segment with a bigger portion of medullar tissue in which the tissue vascularization is extremely contrasted. The red oval in Fig. 3(*a*) indicates the transversal section of two vessels, further shown in the extracted consecutive slices

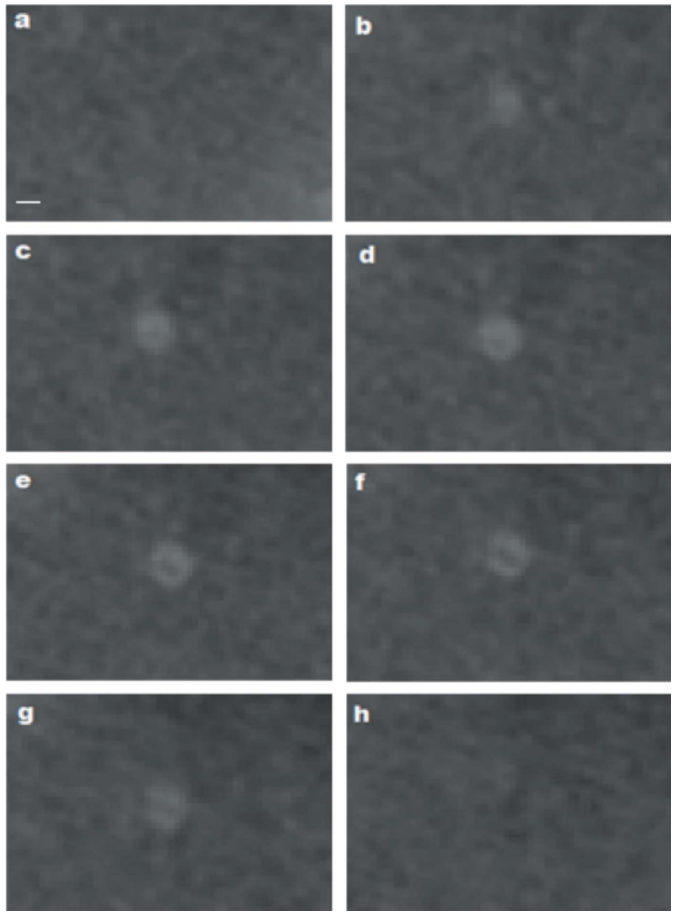


**Figure 2**
Laboratory microCT reconstructed slices with identification extracted every 5 µm depth from a sub-region (highlighted with the red oval in Fig. 1) of the tomography reconstruction where a follicle can be identified. Scale bar: 20 µm.

[Figs. 3(*b*)–3(*e*)] to better highlight their structures. Those slices were extracted at various depths at intervals of 50 µm. Fig. 4(*a*) depicts a longitudinal 3D reconstruction of the tissue from where the identified vessel is virtually extracted and isolated [Fig. 4(*b*)], allowing its overall anatomy to be appreciated. The reconstructed feature is of cylindrical shape with approximate dimension of 60 µm diameter and 0.9 mm length. Fig. 5 is a further transversal section of the reconstructed tissue, showing a different region of the specimen in which we recognize a spherical structure of 40 µm in diameter in the cortex, characterized by a circular bright area with a dark centre, that could be a primordial (or primary) follicle (inside the red circle). As for patient 1 of Fig. 1, this sample was collected from a patient with low ovarian reserve. The total amount of remaining follicles is limited (Wallace & Kelsey, 2010) and is mainly of immature stages (primordial and primary; data not shown). Few follicles have been identified by CT reconstructions in this sample and the one in Figs. 5 and 6 is one of the best examples. Despite the setup of the synchrotron scan being optimized for the visualization of vessels, some follicles were visible as well. Indeed, Fig. 6 depicts magnified images of subsequent slices taken inside the red circle of Fig. 5,

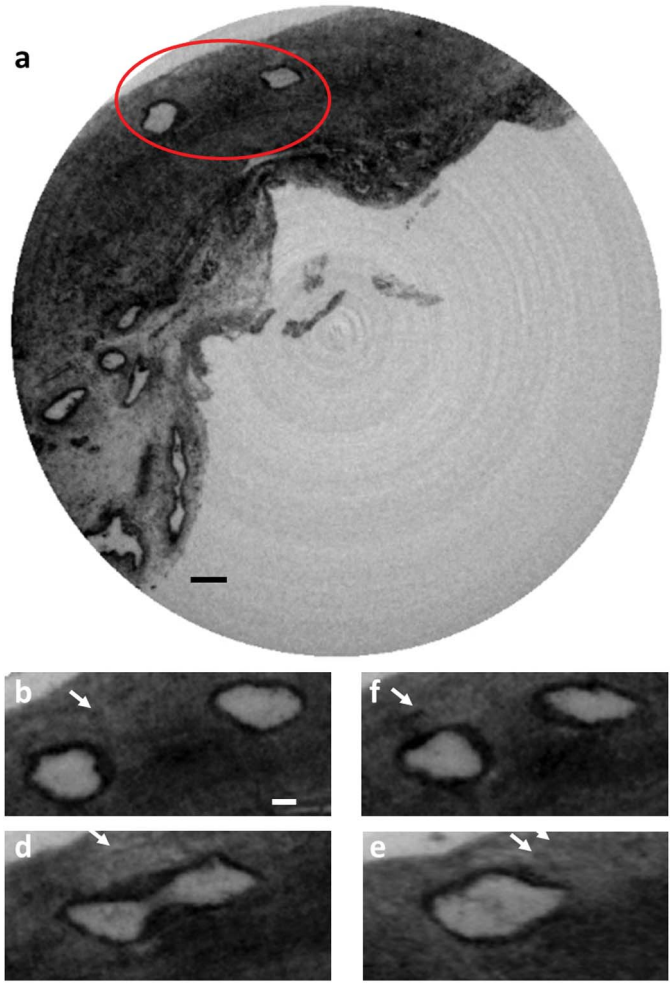


**Figure 3**
(*a*) Slice extracted from the SR-PC microtomography reconstruction. Scale bar: 50 µm. The red oval highlights the presence of two vessels in the cortex. (*b*)–(*e*) Details from the sub-region identified in the red oval, visualizing slices extracted every 50 µm in depth showing the union of the vessels into a bigger vessel. Scale bar: 20 µm.

allowing to identify the rounded shape of the follicle (see arrows) and the progressive appearance of the central nucleus.

### 3.3. STXM

Fig. 7 shows STXM images (absorption and differential phase contrast images) of vessels in a 1.5 µm-thick slice of the ovarian tissues of patient 2. Absorption images are microradiographs sensitive to changes in thickness and/or density of the sample; therefore they provide contrast according to such changes. Differential phase contrast images instead highlight borders and/or structures inside the mapped area (Gianoncelli *et al.*, 2006). According to the direction of the slice cut in the tissue the vessel may appear with different shapes, from elongated [Figs. 7(*a*)–7(*c*)] to semi-round or oval [Figs. 7(*d*)–7(*f*)]. The sub-micrometric resolution of the TwinMic microscope allows typical ovarian stromal cells to be identified as well as blood cells (asterisks) that appear darker (particularly the stromal nucleus) in the absorption images [Figs. 7(*a*) and 7(*d*)]. In Fig. 7(*d*), similarly to that obtained by tomography at higher energy, the vessel lumen (endothelial cells) appears more and uniformly absorbing, and therefore with higher density, compared with the surrounding stroma.

Fig. 8 shows the morphology of an ovarian tissue region [(*a*)–(*c*)] containing primordial follicles [(*d*)–(*i*)]. The high resolution of the STXM images allows the follicular cells to be clearly visualized, as well as the ooplasmic and nuclear structures. As previously shown, the presence of osmium, which specifically stains membranes, together with a proper sample thickness, assures maximal differentiation in absorption and phase contrast images (Gianoncelli *et al.*, 2018).

Figs. 7 and 8 have the advantage of providing high-resolution details of the tissue and the follicles. Such details are not visible with such a high definition by X-ray tomography; some can be guessed from the reconstructed tomographic slices. However, STXM provides a bi-dimensional view of the sample, thus a projection in the direction of the tissue slicing, and therefore it allows for a limited view of the sample. On the

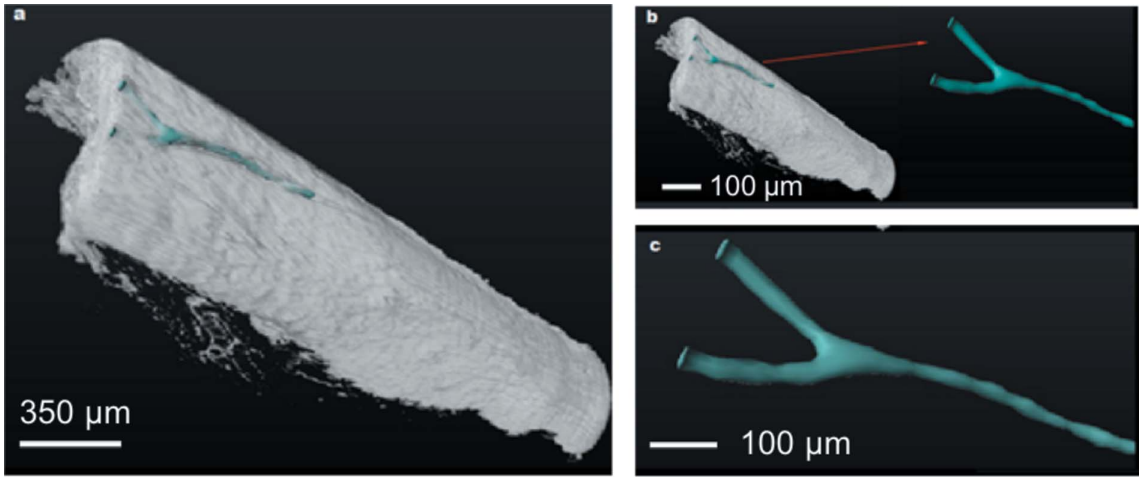


**Figure 4**
(*a*) 3D-volume rendering of the biopsy analysed by SR-PC tomography, together with an extrapolation of the vessel (in blue) (*b*, *c*).

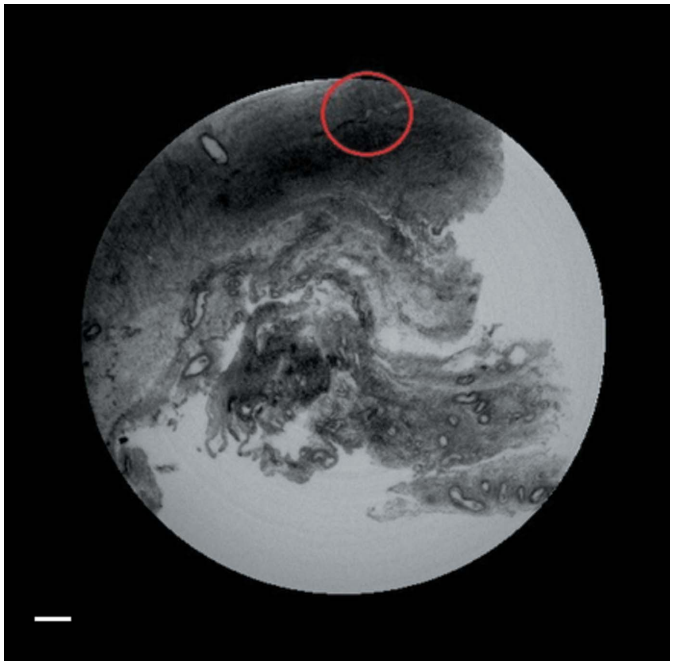

**Figure 5**
Transversal section of the reconstructed tissue by SR-PC tomography, showing a different region of the specimen. The red circle delineates a region in the cortex where we extracted the slices depicted in Fig. 6. Scale bar: 50 µm.

other hand, tomography allows bigger areas to be visualized and in a three-dimensional modality, but with lower spatial resolution.

## 4. Conclusions

In summary, conventional laboratory microCT provides a fast and accessible imaging tool for visualizing human tissues such as the ovary, in a three-dimensional way, providing sufficient resolution to distinguish for instance ovarian cortex from the highly vascularized medulla. Synchrotron-based microCT, on the other hand, can exploit phase contrast which improves image quality due to the strong enhancement between different regions. This allows visualisation of structures deep in the ovarian tissue, even early stage (primordial and primary) ovarian follicles, and vascularity with a higher definition. The drawback, as for all synchrotron techniques, is that access to such facilities is difficult and subject to a peer review system. Moreover, we showed that a deeper understanding of the ovary morphology can be obtained by combining microCT with the STXM soft X-ray microscopy technique which provided us with absorption and differential phase contrast umages at sub-micrometre length scales.

The proposed approach could help to unravel important aspects of human ovarian micro-anatomy (follicles and vessels spatial three-dimensional distribution) and help in fertility preservation research. This type of analysis could be helpful in assisting cryopreservation protocols of ovarian tissue, by analysing the structural damages secondary to those techniques, contributing in improving the current clinical cryopreservation methods (Pascolo, Venturin, Gianoncelli, Salomé *et al.*, 2018; Pascolo, Venturin, Gianoncelli, Bortul *et al.*, 2018; Corral, Clavero *et al.*, 2018), thus enhancing the quality of transplanted follicles and the fertilizing potential.

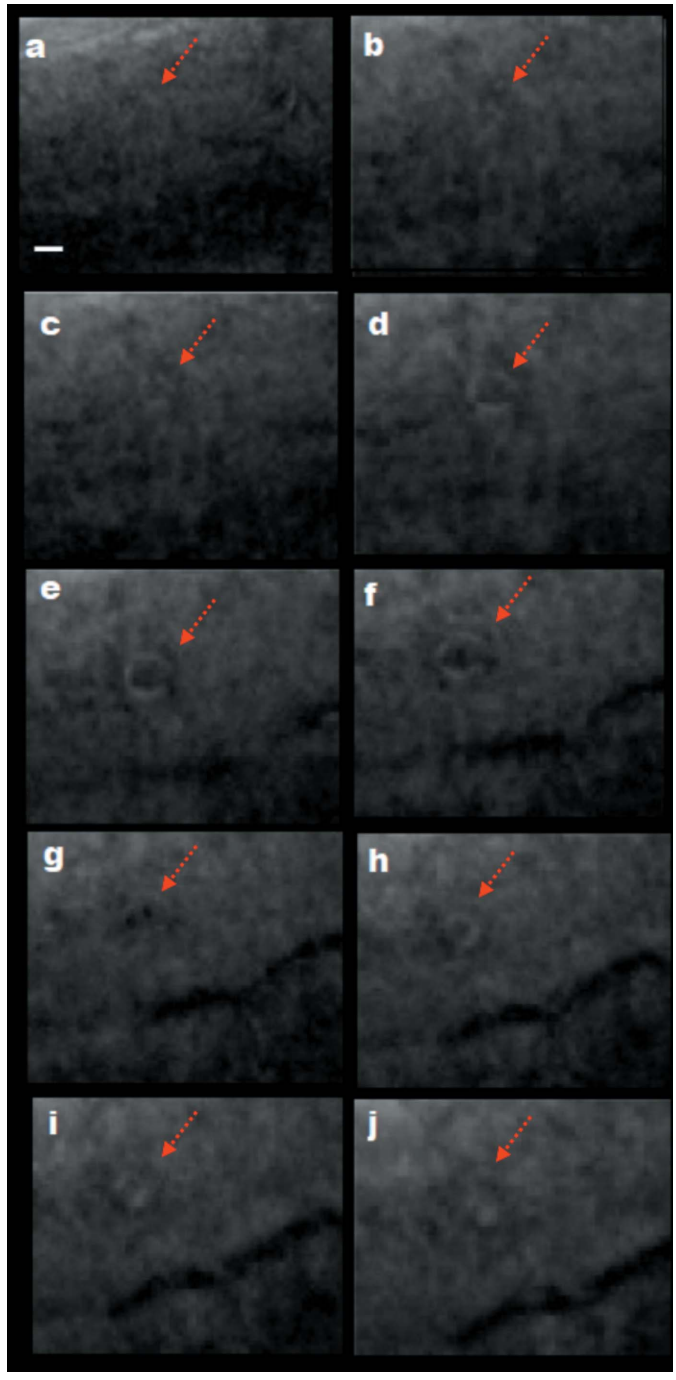


**Figure 6**
Sequential slices (extracted from the area delimited by the red circle in Fig. 5) showing the appearance of a spherical structure of 40 µm in diameter (see arrows), with a hypodense periphery and hyperdense nucleus, compatible with a primordial follicle. Scale bar: 20 µm.

The conventional way to assess follicle quality is based on the use of visible and TEM microscopies, after a suitable sample preparation which includes, in the case of TEM, osmium staining and tissue slicing. Our results proves that

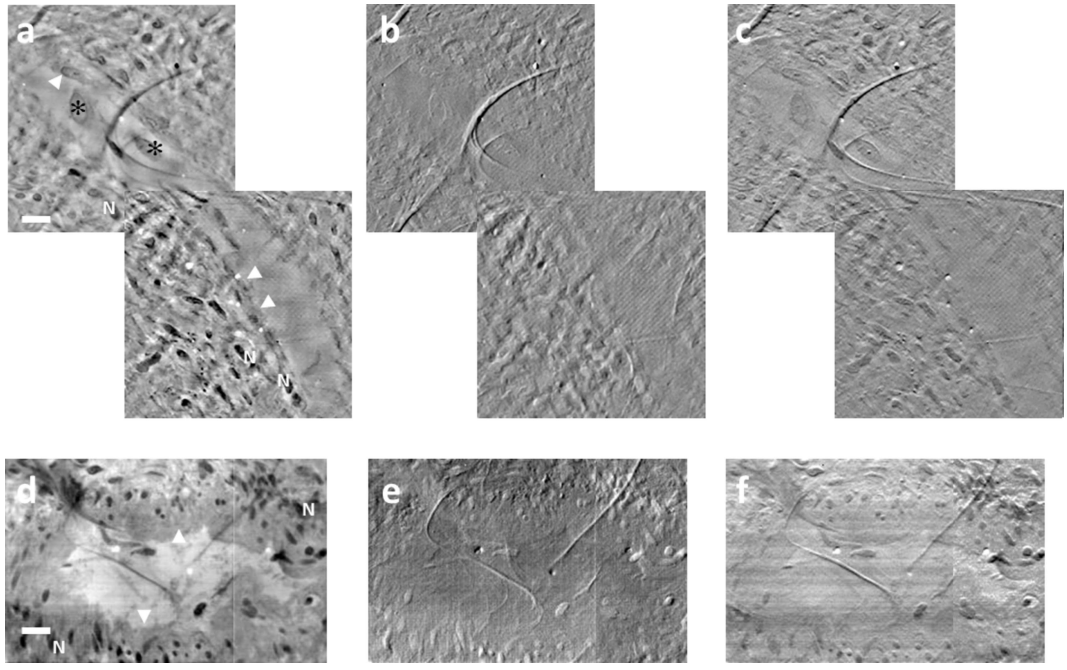


**Figure 7**
(*a*) STXM images, absorption (*a*,*d*), differential phase contrast in the *x* direction (*b*,*e*) and differential phase contrast in the *y* direction (*c*,*f*) of two vessels in a fresh tissue slice. Vessels' walls are indicated by white tringles, red blood cells by asterisks and the nuclei of stromal cells by N. Images acquired at the TwinMic beamline (Elettra Sincrotrone Trieste) at 1 keV with 250 nm spot size. Scale bar: 10 µm.

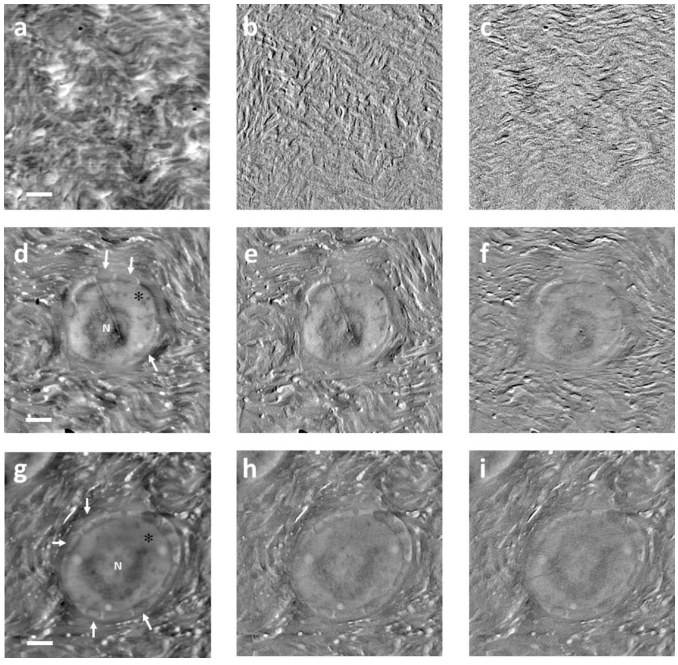


**Figure 8**
STXM images, absorption (*a*,*d*, *g*), differential phase contrast in the *x* direction (*b*,*e*,*h*) and differential phase contrast in the *y* direction (*c*,*f*,*i*) of a fresh tissue area (*a*, *b*,*c*) and two follicles (*d*,*e*,*f* and *g*,*h*,*i*) in a fresh tissue slice. The granulosa cells of the follicles are indicated in the images by arrows, ooplasm by asterisks (*) and the nuclei of stromal cells by N. Images acquired at the TwinMic beamline (Elettra Sincrotrone Trieste) at 1 keV with 250 nm spot size. Scale bar: 10 µm.

osmium staining provides a good contrast also in the X-ray micrographs both at low and high X-ray energy; although it is expected that absorption imaging would benefit from osmium staining, it appears that this dye assists properly also in phase contrast modality.

Moreover, embedding in epoxy resin, normally used for TEM samples, proved to be a suitable material also for 3D X-ray imaging.

The manuscript reports the analyses on a limited number of samples obtained from the human ovarian cortex of two patients. It aims at demonstrating how microCT can become a powerful tool for a better knowledge of the structure of human ovary.

## Acknowledgements

Financial support by Health Ministry (RF-2011-02351812) Ricerca Finalizzata 'Applications of Ultrastructural Cell Analysis in the Field of Reproductive Technologies' is gratefully acknowledged. This work was also supported by a grant from the Institute for Maternal and Child Health IRCCS Burlo Garofolo (Trieste, Italy). GS acknowledges the STEP ICTP program and the ICTP-Elettra Users Programme support.

## Funding information

The following funding is acknowledged: STEP ICTP program; ICTP-Elettra Users Programme support.

## References


Amorim, C. A. & Shikanov, A. (2016). *Future Oncol.* **12**, 2323–2332.

Arfelli, F., Assante, M., Bonvicini, V., Bravin, A., Cantatore, G., Castelli, E., Dalla Palma, L., Di Michiel, M., Longo, R., Olivo, A., Pani, S., Pontoni, D., Poropat, P., Prest, M., Rashevsky, A., Tromba, G., Vacchi, A., Vallazza, E. & Zanconati, F. (1998). *Phys. Med. Biol.* **43**, 2845–2852.

Betz, O., Wegst, U., Weide, D., Heethoff, M., Helfen, L., Lee, W.-K. & Cloetens, P. (2007). *J. Microsc.* **227**, 51–71.

Boerckel, J. D., Mason, D. E., McDermott, A. M. & Alsberg, E. (2014). *Stem Cell. Res. Ther.* **5**, 144.

Bravin, A., Coan, P. & Suortti, P. (2013). *Phys. Med. Biol.* **58**, R1–R35.

Brun, F., Pacilè, S., Accardo, A., Kourousias, G., Dreossi, D., Mancini, L., Tromba, G. & Pugliese, R. (2015). *Fund. Inform.* **141**, 233–243.

Bukovsky, A., Caudle, M. R., Svetlikova, M. & Upadhyaya, N. B. (2004). *Reprod. Biol. Endocrinol.* **2**, 20.

Chiti, M. C., Dolmans, M. M., Donnez, J. & Amorim, C. A. (2017). *Ann. Biomed. Eng.* **45**, 1650–1663.

Chiti, M. C., Dolmans, M.-M., Hobeika, M., Cernogoraz, A., Donnez, J. & Amorim, C. A. (2017). *J. Ovarian Res.* **10**, 71.

Chiti, M. C., Dolmans, M.-M., Mortiaux, L., Zhuge, F., Ouni, E., Shahri, P. A. K., Van Ruymbeke, E., Champagne, S.-D., Donnez, J. & Amorim, C. A. (2018). *J. Assist. Reprod. Genet.* **35**, 41–48.

Chiti, M. C., Donnez, J., Amorim, C. A. & Dolmans, M.-M. (2018). *Minerva Ginecol.* **70**, 444–455.

Cloetens, P., Barrett, R., Baruchel, J., Guigay, J.-P. & Schlenker, M. (1996). *J. Phys. D Appl. Phys.* **29**, 133–146.

Corral, A., Balcerzyk, M., Gallardo, M., Amorim, C. A., Parrado-Gallego, Á. & Risco, R. (2018). *Theriogenology*, **119**, 183–188.

Corral, A., Clavero, M., Gallardo, M., Balcerzyk, M., Amorim, C. A., Parrado-Gallego, Á., Dolmans, M.-M., Paulini, F., Morris, J. & Risco, R. (2018). *Cryobiology*, **81**, 17–26.

Davis, T. J., Gao, D., Gureyev, T. E., Stevenson, A. W. & Wilkins, S. W. (1995). *Nature*, **373**, 595–598.

De Caro, L., Cedola, A., Giannini, C., Bukreeva, I. & Lagomarsino, S. (2008). *Phys. Med. Biol.* **53**, 6619–6637.

Fitzgerald, R. (2000). *Phys. Today*, **53**, 23–26.

Gianoncelli, A., Kourousias, G., Altissimo, M., Bedolla, D. E., Merolle, L., Stolfa, A. & Shin, H.-J. (2016). *AIP Conf. Proc.* **1764**, 030002.

Gianoncelli, A., Kourousias, G., Merolle, L., Altissimo, M. & Bianco, A. (2016). *J. Synchrotron Rad.* **23**, 1526–1537.

Gianoncelli, A., Kourousias, G., Zweyer, M., Ricci, G. & Pascolo, L. (2018). *Nucl. Instrum. Methods Phys. Res. A*, https://doi.org/10.1016/j.nima.2018.09.070.

Gianoncelli, A., Morrison, G. R., Kaulich, B., Bacescu, D. & Kovac, J. (2006). *Appl. Phys. Lett.* **89**, 251117.

Kim, J., Choi, Y. H., Chang, S., Kim, K.-T. & Je, J. H. (2012). *Sci. Rep.* **2**, 468.

Ladanyi, C., Mor, A., Christianson, M. S., Dhillon, N. & Segars, J. H. (2017). *J. Assist. Reprod. Genet.* **34**, 709–722.

Laronda, M. M., Rutz, A. L., Xiao, S., Whelan, K. A., Duncan, F. E., Roth, E. W., Woodruff, T. K. & Shah, R. N. (2017). *Nat. Commun.* **8**, 15261.

Makabe, S., Naguro, T. & Stallone, T. (2006). *Microsc. Res. Tech.* **69**, 436–449.

Mayo, S., Davis, T., Gureyev, T., Miller, P., Paganin, D., Pogany, A., Stevenson, A. & Wilkins, S. (2003). *Opt. Express*, **11**, 2289–2302.

Metscher, B. D. (2009). *BMC Physiol.* **9**, 11.

Mizutani, R., Takeuchi, A., Uesugi, K., Takekoshi, S., Osamura, R. Y. & Suzuki, Y. (2010). *Cereb. Cortex*, **20**, 1739–1748.

Morrison, G. R., Gianoncelli, A., Kaulich, B., Bacescu, D. & Kovac, J. (2006). *Proceedings of the 8th International Conference on X-ray Microscopy, IPAP Conf. Series 7*, pp. 377–379.

Paganin, D., Mayo, S. C., Gureyev, T. E., Miller, P. R. & Wilkins, S. W. (2002). *J. Microsc.* **206**, 33–40.

Pascolo, L., Venturin, I., Gianoncelli, A., Bortul, R., Zito, G., Giolo, E., Salomé, M., Bedolla, D. E., Altissimo, M., Zweyer, M. & Ricci, G. (2018). *Reprod. Biomed. Online.* **37**, 153–162.

Pascolo, L., Venturin, I., Gianoncelli, A., Salomé, M., Altissimo, M., Bedolla, D. E., Giolo, E., Martinelli, M. S., Luppi, S., Romano, F., Zweyer, M. & Ricci, G. (2018). *J. Instrum.* **13**, C06003.

Paulini, F., Chaves, S. B., Rôlo, J. L. J. P., Azevedo, R. B. D. & Lucci, C. M. (2017). *An. Acad. Bras. Cienc.* **89**, 2131–2139.

Pogany, A., Gao, D. & Wilkins, S. W. (1997). *Rev. Sci. Instrum.* **68**, 2774–2782.

Ritman, E. L. (2011). *Annu. Rev. Biomed. Eng.* **13**, 531–552.

Rozenblit, A. M., Ricci, Z. J., Tuvia, J. & Amis, E. S. (2001). *Am. J. Roentgenol.* **176**, 119–122.

Saksouk, F. A. & Johnson, S. C. (2004). *Radiogr. Rev. Publ. Radiol. Soc. N. Am. Inc.* pp. **24**(Suppl. 1), S133–S146.

Tromba, G., Longo, R., Abrami, A., Arfelli, F., Astolfo, A., Bregant, P., Brun, F., Casarin, K., Chenda, V., Dreossi, D., Hola, M., Kaiser, J., Mancini, L., Menk, R. H., Quai, E., Quaia, E., Rigon, L., Rokvic, T., Sodini, N., Sanabor, D., Schultke, E., Tonutti, M., Vascotto, A., Zanconati, F., Cova, M., Castelli, E. & Siu, K. K. W. (2010). *AIP Conf. Proc.* **1266**, 18–23.

Wallace, W. H. B. & Kelsey, T. W. (2010). *PLoS One*, **5**, e8772.

Wilkins, S. W., Gureyev, T. E., Gao, D., Pogany, A. & Stevenson, A. W. (1996). *Nature*, **384**, 335–338.

Williams, C. J. & Erickson, G. F. (2000). *Endotext*, edited by L. J. De Groot, G. Chrousos, K. Dungan, K. R. Feingold, A. Grossman, J. M. Hershman, C. Koch, M. Korbonits, R. McLachlan, M. New, J. Purnell, R. Rebar, F. Singer & A. Vinik. South Dartmouth: MDText.com, Inc.